A Non-classical Dihydrogen Adduct of S = ½ Fe(I)

Yunho Lee,[†§] R. Adam Kinney,[‡] Brian M. Hoffman*,[‡] and Jonas C. Peters*,[†]
[†]Division of Chemistry and Chemical Engineering, California Institute of Technology, Pasadena, California 91125 (USA),
[‡]Department of Chemistry, Northwestern University, 2145 Sheridan Road, Evanston, Illinois 60208 (USA) and
[§]Present address: Department of Chemistry, Korea Advanced Institute of Science and Technology (KAIST), Daejeon 305-701 (Korea)

Contents

Experimental Section.
Figure S1. ^{1}H-NMR spectra of the reaction of **2** with H_2(g) in C_6D_6.
Figure S2. ^{1}H-NMR spectra of the reaction of **2** with H_2(g) in toluene-d_8.
Figure S3. UV-Vis spectra and near IR of $(SiP^{iPr}_3)Fe(H_2)$ (**3**) and $(SiP^{iPr}_3)Fe(N_2)$ (**2**) in toluene.
Figure S4. React IR spectra of the reaction of $(SiP^{iPr}_3)Fe(N_2)$ (**2**, red spectra) with H_2 (g) in THF.
Figure S5. ^{1}H-NMR spectra of **3** in C_6D_6; (a) in-situ generated **3** (b) a powder sample of **3** dissolved in C_6D_6.
Figure S6. ^{1}H-NMR spectra of the reaction of **3-D$_2$** under D_2 (g) in C_6D_6.
Figure S7. ^{2}H-NMR spectra of **3-D$_2$** in toluene-d_8 at –70°C.
Figure S8. ^{1}H-NMR spectra of the reaction of **2** with HD (g) in C_6D_6.
Figure S9. Solid-state structure of $(SiP^{iPr}_3)Fe(H_2)$ (**3**) obtained from the benzene solution of **3** under the vacuum for several weeks.
Figure S10. Solid-state structure of **3** obtained from the saturated benzene solution of **3** under the H_2 atmosphere for several days.
Figure S11. X-band EPR data of (A) **2**, (B) **3**, (C) **3′** and (D) a mixture of **2** and **3** in THF/2-MeTHF (9/1) at 77 K.
Figure S12. X-band EPR data of **3′** in 9:1 THF/2-MeTHF (blue line) and in toluene (red line) at 20 K.
Figure S13. X-band EPR spectra of **2**, **3** and **3′** in toluene at 20 K.
Figure S14. X-band EPR spectra, with simulation, of **2** in toluene at 20 K.
Figure S15. X-band EPR spectra of **3**, with simulation, in toluene at 20 K.
Figure S16. X-band EPR spectra of **3′**, with simulation, in toluene at 20 K.
Figure S17. EPR spectra of **3** in frozen solution (35 GHz and 9 GHz), and in powder (9 GHz).
Figure S18. 2D field-frequency ^{1}H ENDOR pattern of **3** in frozen solution with ENDOR simulations corresponding to $\beta = 0^o$, 15^o, and 30^o.
Figure S19. Single crystal EPR analysis of **3**
Figure S20. ^{1}H PESTRE traces of **3** at g_2.
Figure S21. 2D field-frequency ^{2}H ENDOR pattern of **3′** in frozen solution with ENDOR simulations.
Figure S22. DFT optimized geometries of **3** and FeH^-/SiH^+.

Figure S23. ^{1}H-NMR spectra of **4** (top), {(SiP$^{i\mathrm{Pr}}_3$)Fe(THF-d_8)}{B(3,5-(CF$_3$)$_2$-C$_6$H$_3$)$_4$} (middle), and **5** (bottom) in C$_6$D$_6$/THF-d_8 (4/1) at room temperature.
Figure S24. ^{1}H-NMR spectra of A: **4**, B: with N$_2$/H$_2$ (5:1), C: with N$_2$/H$_2$ (1:1), D: with N$_2$/H$_2$ (1:5) and E: **5** in C$_6$D$_6$/THF-d$_8$ (4/1) at room temperature.
Figure S25. UV-Vis spectra of a series of {(SiP$^{i\mathrm{Pr}}_3$)Fe(L)}{B(3,5-(CF$_3$)$_2$-C$_6$H$_3$)$_4$}; L = N$_2$ (**4**), THF, and H$_2$ (**5**) in THF at room temperature.
Figure S26. UV-Vis spectrum (nm {cm^{-1}M^{-1}}) of {(SiP$^{i\mathrm{Pr}}_3$)Fe(N$_2$)}{B(3,5-(CF$_3$)$_2$-C$_6$H$_3$)$_4$} (**4**), green spectra: 613 {260}, 757 {330}) in diethyl ether at room temperature.
Figure S27. ^{1}H-NMR spectrum of **6** in toluene-d_8 at RT.
Figure S28. ^{15}N-NMR spectrum of **6** with ^{31}P-decoupling measured at 293 K.
Figure S29. Variable temperature ^{31}P-NMR spectra of **6** in toluene-d_8.
Figure S30. ^{31}P-NMR spectrum of **6** in toluene-d_8 at –90°C.
Figure S31. Solid-state structure of (SiP$^{i\mathrm{Pr}}_3$)Fe(N$_2$)(H) (**6**).

Experimental Section.

General Considerations. All manipulations were carried out using standard Schlenk or glovebox techniques under a N_2 atmosphere. Unless otherwise noted, solvents were deoxygenated and dried by thoroughly sparging with Ar gas followed by passage through an activated alumina column in a solvent purification system by SG Water, USA LLC. Non-halogenated solvents were tested with a standard purple solution of sodium benzophenone ketyl in tetrahydrofuran in order to confirm effective oxygen and moisture removal. $HSiP^{i}Pr_3$,[1] $(SiP^{i}Pr_3)Fe(CH_3)$, [2] $(SiP^{i}Pr_3)Fe(N_2)$,2 $\{(SiP^{i}Pr_3)Fe(N_2)\}$ $\{B(3,5\text{-}(CF_3)_2\text{-}C_6H_3)_4\}2$ and $H(OEt_2)_2\{B(3,5\text{-}(CF_3)_2\text{-}C_6H_3)_4\}$[3] were prepared according to literature procedures. All reagents were purchased from commercial vendors and used without further purification unless otherwise stated. Elemental analyses were performed by Midwest Microlab, LLC., Indianapolis, IN. Deuterated solvents were purchased from Cambridge Isotope Laboratories, Inc., degassed, and dried over activated 3-Å molecular sieves prior to use.

X-ray Crystallography Procedures. X-ray diffraction studies for **3**[4] and **6** were carried out at the MIT Department of Chemistry X-Ray Diffraction Facility on a Bruker three-circle Platform diffractometer, equipped with a CCD detector. XRD study for **3**[5] was carried out at the Beckman Institute Crystallography Facility at Caltech on a Bruker Kappa Apex II diffractometer. Data was collected at 100 K using Mo Kα (λ = 0.71073 Å) or Cu Kα (λ = 1.54178 Å) radiation and solved using SHELX version 6.14.[6] X-ray quality crystals were grown as described in the experimental procedures. The crystals were mounted on a glass fiber or nylon loop with Paratone N oil. Structures were determined using direct methods with standard Fourier techniques using the Bruker AXS software package.

Spectroscopic measurements. Varian Mercury-300, Inova-500 and Bruker AVANCE-400 spectrometers were used to record ^{1}H, and ^{31}P NMR spectra at ambient temperature unless otherwise indicated. ^{1}H chemical shifts were referenced to residual solvent peaks. ^{31}P chemical shifts were referenced to external phosphoric acid (δ = 0 ppm). Solution magnetic moments were determined by the method of Evans.[7,8] Optical spectroscopy measurements were taken on a Cary 50 UV-Vis spectrophotometer using a 1-cm two-window quartz cell sealed with a standard closed cap purchased from Starna Cells, Inc (Catalog number: 1-Q-10-GL14-C). Infrared spectra were recorded on a BioRad FTS 3000 EXCALIBUR series FT-IR spectrometer. X-band EPR spectroscopy measurements were taken on a Bruker EMS spectrometer. The solution samples of **2**, **3**, and **3′** were prepared with THF/2-MeTHF (9/1) or toluene. The preparation of **3** and **3′** samples was conducted inside the glovebox under N_2 atmosphere by transferring the corresponding solution into an EPR tube. The temperature of the samples was maintained below –90°C followed by immediately freezing the sample with liquid nitrogen. The single crystal sample of **3** for EPR analysis was prepared inside a J-young EPR tube in the glovebox and degassed thorough three freeze-pump-thaw cycles on the Schlenk line followed by charging with

[1] Mankad, N. P.; Whited, M. T.; Peters, J. C. *Angew. Chem. Int. Ed.* **2007**, *46*, 5768-5771.
[2] Lee, Y., Mankad, N. P., Peters, J. C. *Nature Chem.* **2007**, *2*, 558-565.
[3] Yakelis, N. A.; Bergman, R. G. *Organometallics* **2005**, *24,* 3579-3581. Brookhart, M.; Grant, B.; Volpe, Jr, A. F. *Organometallics* **1992**, *11*, 3920-3922.
[4] Obtained from a crystal grown under full vacuum.
[5] Obtained from a crystal grown under H_2 atmosphere.
[6] Sheldrick, G. M. *Acta Cryst. A* , **2008**, *64*, 112.
[7] Evans, D. F. *J. Chem. Soc*, **1959**, 2003-2005.
[8] Sur, S. K. *J. Magn. Reson.* **1989**, *82*, 169-173.

H_2 (1 atm). Low temperature experiments were carried out via either a continuous-flow He(*l*) cryostat or an N_2(*l*) finger dewar and the collected spectra were simulated using the W95EPR program.[9]

X-band EPR spectra from a single crystal of **3** were collected at 77 K on a modified Varian E-4 EPR spectrometer (**Fig. S22**). Spectra were collected as a single crystal of **3** in an arbitrary orientation was rotated 180° in a single plane in 10° increments; 0° corresponds to an arbitrary starting direction that is perpendicular to B_o. We observe only a single EPR resonance for all orientations of the crystal, as expected from the crystal structure of **3** which contains one Fe center per unit cell The data is analyzed according to the methodology described in Gurbiel, et al.[10] This analysis confirms that the g values describing **3** in frozen solution correctly describe the paramagnetic complex in the single crystal. This unambiguously demonstrates that **3** in frozen solution and in a single crystal samples are the same species.

35 GHz CW and pulse EPR and ENDOR spectroscopic data were collected on home-built spectrometers, described previously,[11] that were equipped with liquid helium immersion dewars for measurements at 2 K. The CW measurements employed 100 kHz field modulation and dispersion mode detection under rapid passage conditions. ^{1}H CW ENDOR spectra employed broadening of the RF to 100 kHz to improve signal-to-noise.[12] ^{1}H CW ENDOR spectra were collected using the stochastic-field modulation detected ENDOR sequence, as previously described,[13] to improve ENDOR lineshapes. Pulsed ^{1}H ENDOR spectra were collected with the Davies microwave pulse sequence: π - T - $\pi/2$ - τ - π - τ - echo, where T is the time interval during which the RF pulse is applied.[14] Data acquisition for all pulse experiments utilized the SpecMan software package (http://specman.4epr.com) in conjunction with a Spin-Core PulseBlaster ESR_PRO 400 MHz word generator and an Agilent Technologies Acquiris DP235 500MS/sec digitizer.

For a single molecular orientation and for nuclei with a nuclear spin of I = 1/2 (^{1}H), the ENDOR transitions for the $m_s = \pm 1/2$ electron manifolds are observed at frequencies dictated by the equation

$$\nu_{\pm} = |\nu_n \pm A/2|$$

where ν_n is the nuclear Larmor frequency and A is the orientation-dependent hyperfine coupling. For I ≥ 1 (^{2}H), the two ENDOR lines are further split by the orientation-dependent nuclear quadrupole interaction (3P). The peaks are then observed at frequencies dictated by a modified version of the equation above:

$$\nu_{\pm,\pm} = |\nu_{\pm} \pm 3P/2|$$

Signs of the hyperfine couplings measured from ENDOR spectra (more specifically, the sign of g_{Nuc}/A_{Nuc}) have been obtained by application of the Pulse-Endor-SaTuration-REcovery (PESTRE) protocol, a pulse sequence comprised of multiple Davies ENDOR sequences, carried out in three distinct experimental phases: (I) an EPR saturation phase (RF off) of 100 Davies sequences whose spin-echo intensities quickly converge to the steady-state 'baseline' (BSL); (II) an ENDOR perturbation phase of 24 sequences, in which each sequence contains a fixed RF set

---

[9] Neese, F. *QCPE Bull.* **1995**, *15*, 5.

[10] Gurbiel, R.J., et al., *J. Mag. Res.*, **1991**, 91, 227-240.

[11] (a) Werst, M.M., Davoust, C.E., Hoffman, B.M., *J. Am. Chem. Soc.*, **1991**, 113(5), 1533-1538. (b) Davoust, C. E.; Doan, P. E.; Hoffman, B. M., *J. Magn. Reson.*, **1996**, 119, 38-44. (c) Zipse, H.; Artin, E.; Wnuk, S.; Lohman, G. J. S.; Martino, D.; Griffin, R. G.; Kacprzak, S.; Kaupp, M.; Hoffman, B.; Bennati, M.; Stubbe, J.; Lees, N., *J. Am. Chem. Soc.*, **2009**, 131, 200-211.

[12] Hoffman, B. M.; DeRose, V. J.; Ong, J. L.; Davoust, C. E. *J. Magn. Reson.* **1994**, 110, 52-57.

[13] Lee, H.I., *et al.*, *J. Am. Chem. Soc.*, **2004**, 126, 9563-9569.

[14] Schweiger, A., Jeschke, G., *Principles of Pulsed Electron Paramagnetic Resonance*; Oxford University Press: Oxford, U.K., 2001; p 578.

at one or the other of the branches of the ENDOR spectrum ($\nu_{\pm}$); (III) and an EPR recovery phase (RF off) of 132 sequences during which the spin echo corresponds to the spin-echo 'dynamic reference level' (drl) associated with ENDOR-induced spin polarization created in the second phase, with the *drl* relaxing to the BSL during this phase. In the slow-relaxation regime, the sign of A_{Nuc} is unambiguously given by the sign of the difference between the drl and BSL echo intensities as observed for either ENDOR branch. When $A_{Nuc} > 0$ (and $g_{Nuc} > 0$): if ν_+ is being interrogated, the *drl* relaxes to the BSL from below; when ν_- is being interrogated, the *drl* relaxes to the BSL from above. When $A_{Nuc} < 0$, the opposite behavior is observed.[15]

DFT Calculations. Density function calculations were performed with the Amsterdam Density Functional (ADF) software package (ADF version 2010.01, SCM, Theoretical Chemistry, Vrije Universitait, Amsterdam, The Netherlands.). Geometry optimization calculations on **3** and on the proposed product of heterolytic cleavage of H_2 (denoted FeH^-/SiH^+) were performed with a BLYP functional in the spin-unrestricted formalism (spin polarization 1), using a TZ2P basis set with a small frozen core potential. The starting geometry for the $[SiP^{iPr}_3]Fe(I)$ complex in all calculations consisted of the solid state structure of **3** obtained under an H_2 atmosphere, as presented herein. The entire $[SiP^{iPr}_3]^-$ ligand was used for all geometry optimization calculations.

Geometry optimization of the hypothetical product obtained from heterolytic cleavage of H_2 reveals an increase in the distance between Fe and Si of approximately 1 Å relative to both the solid state structure and the DFT optimized structure of **3** (r(FeSi) = 2.247 and 2.267 Å for the solid state and DFT optimized structures, respectively). The energy of FeH^-/SiH^+ is calculated at +62 kcal/mol (2.6 eV) higher in energy relative to the calculated H_2 adduct. We note that attempts to model a di-hydride product, the product expected from oxidative addition of H_2, resulted in a minimized geometry that was nearly identical to that obtained from the calculation starting from an H_2 adduct, with nearly identical energies (ΔE = 4 kcal/mol).

$(SiP^{iPr}_3)Fe^I(H_2)$ (3). In a NMR tube with J-young valve the red C_6D_6 solution of **2** was degassed by three freeze-pump-thaw cycles on the Schlenk line. After H_2 gas (1 atm) was added the reaction mixture was heated at 60°C for 6 hrs or shaking at room temperature (5-6 hrs). ^{1}H-NMR reveals disappearance of **2** and the formation of $(SiP^{iPr}_3)Fe^I(H_2)$ (**3**) which can be isolated as an orange powder. Completion of the reaction was accomplished by repetition (typically over 3 times) of the degassing procedure followed by addition of H_2 (g) until complete disappearance of **2** was observed as monitored by ^{1}H-NMR. ^{1}H-NMR (C_6D_6, ppm): 8.0, 7.0, 6.25, 4.47(H_2), 3.73, ~1.5. μ_{eff} (C_6D_6, 20°C): 1.88 μ_B {$(SiP^{iPr}_3)Fe^I(N_2)$ (**2**): 1.90 μ_B and $(SiP^{iPr}_3)Fe^I(CO)$: 1.86 μ_B}. Crystals suitable for X-ray diffraction were obtained by slow evaporation of benzene from a saturated solution of **3** under full vacuum or slow cooling of a saturated benzene solution of **3** under H_2 atmosphere. Elemental analysis was not accomplished due to the high sensitivity of **3** toward N_2. UV-Vis (toluene, nm {$cm^{-1}M^{-1}$}): 290 {8,200}, 380 {4,450}, 1,350 {100}. IR (KBr pellet; cm^{-1}): 2908 (H_2), (THF solution; cm^{-1}): 2960.

$(SiP^{iPr}_3)Fe^I(H_2)$ (3) isolated as an orange powder. In a 100 ml Schlenk tube a red solution of $(SiP^{iPr}_3)Fe(N_2)$ (**2**, 150 mg, 0.217 mmol) in benzene (30 mL) was degassed by three freeze-pump-thaw cycles on the Schlenk line. After H_2 gas (1 atm) was added the reaction mixture was heated overnight at 60°C. The reaction solution was quickly filtered through Celite and volatiles were removed under vacuum to give an orange powder. The solid was collected on a glass-frit and washed with pentane (3 mL x 1). The resulting product **3** (130 mg, 0.195 mmol, 90%) was obtained as an orange powder after drying under vacuum. Spectroscopic features in the ^{1}H-NMR

[15] Doan, P.E., *J. Mag. Res.*, **2011**, 208, 76-86.

were identical for **3** except **2** was present as a impurity due to the labile H_2 ligand replaced by atmospheric N_2.

(SiP^{iPr}_3)$Fe^{I}(D_2)$ (3′). In a NMR tube with J-young valve a red C_6D_6 or Tol-d_8 solution of **2** was degassed by three freeze-pump-thaw cycles on the Schlenk line. Lithium deuteride (90 mg, 10 mmol) in a 25 ml round bottom flask was taken out of the dry-box and attached to the Schlenk line. Under an N_2 atmosphere degassed D_2O (0.2 ml, 10 mmol) was added to the flask through the side arm at liquid nitrogen temperature. After evacuation of the flask by full vacuum the mixture was slowly warmed to room temperature with stirring. The flask was cooled down to 77 K after the pressure of generated D_2 gas reached to 1 atm as monitored by manometer. After D_2 gas was added the solution was heated at 60°C for 6 hrs or shaken at room temperature for 5-6 hrs and reaction was monitored by ^{1}H-NMR revealing gradual disappearance of **2** and the slow formation of **3′**. Spectroscopic features in the ^{1}H-NMR were almost identical for **3**. ^{1}H-NMR (C_6D_6, ppm): 7.9, 7.0, 6.29, 3.71, ~1.5. No deuterium signal was detected in Tol-d_8 at –70°C.

HD gas experiment. In a NMR tube with J-young valve a red C_6D_6 solution of **2** was degassed by three freeze-pump-thaw cycles on the Schlenk line. Lithium hydride (90 mg, 10 mmol) in a 25 ml round bottom flask was taken out of the dry-box and attached to the Schlenk line. Under an N_2 atmosphere degassed D_2O (0.2 ml, 10 mmol) was added to the flask through the side arm at liquid nitrogen temperature. After evacuation of the flask by full vacuum the mixture was slowly warmed to room temperature with stirring. The flask was cooled down to 77 K after the pressure of generated HD gas reached to 1 atm as monitored by manometer. After HD gas was added to the solution in a NMR tube the solution was shaken at room temperature for 15 hrs and reaction was monitored by ^{1}H-NMR revealing gradual disappearance of **2** and the slow formation of **3-HD**. Spectroscopic features in the ^{1}H-NMR were well matched with those of **3**. ^{1}H-NMR (C_6D_6, ppm): 7.9, 7.0, 6.29, 3.71, ~1.5. The H_2/HD ratio was very slowly changing from 0.12 to 0.17 for 15 hrs.

Equilibrium studies. To accurately determine the equilibrium constants of the corresponding reactions, the solubility of H_2 in the reaction mixture was obtained by the integration of the peak at 4.5 ppm relative to the internal reference mesitylene in C_6D_6 at room temperature. The concentration of N_2 was obtained according to published methodology.[16] We used two different gas mixtures to obtain equilibrium constants in this work, one with 58 ml of N_2 and 57.5 ml of H_2, which gives 23 mM of N_2 and 2.8 mM of H_2 in C_6D_6 at room temperature. The other gas mixture is composed with 293 ml of N_2 and 57.5 ml of H_2, which gives 36 mM of N_2 and 0.76 mM of H_2.

[16] Weare, W. W.; Dai, X.; Byrnes, M. J.; Chin, J. M.; Schrock, R. R.; Müller, P. *Proc. Natl. Acad. Sci.* **2006**, *103*, 17099-17106.

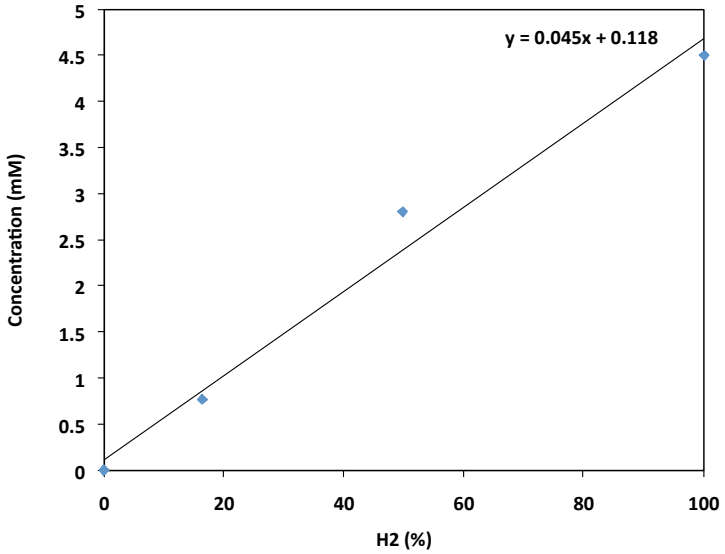

Two glass bulbs connected by a glass joint with a glass stopcock were used to mix H_2 and N_2 gases. The top bulb (measured volume 57.5 ml) is equipped with a glass stopcock and a 24/40 glass joint, which is attached to the Schlenk line. The bottom glass bulb (measured volume 58 ml or 293 ml) is equipped with a 14/20 glass joint which is attached to glass adaptor for a NMR tube with J-young valve. After degassing the corresponding sample solution, the NMR tube was attached to the bottom glass bulb. The two bulbs were completely evacuated by applying a full vacuum for 30 min. The first gas, H_2 was added to the top bulb, while the middle stopcock is closed. Once 1 atm pressure of H_2 was added as confirmed by the manometer, the top stopcock was closed followed by opening the middle stopcock. After the Schlenk line was completely charged with the second gas N_2 by 5 times of vacuum/purge cycles the top stopcock was open. Once 1 atm pressure was reached, the top stopcock was closed. In order to accomplish the complete mixture of two gases, the gas mixture was allowed to stand for 15 min at room temperature. After the gas mixture was added the NMR tube was rotated at 10-15 rpm for 6-12 hrs at room temperature. The reaction was monitored by ^{1}H-NMR spectroscopy and each measurement was conducted with a 6-12 hr interval for 3-10 days. The same procedure was repeated 2-3 times for each data point with omission of the first data point from the calculation for K_{eq}.

Equilibrium studies for the reaction of $(SiP^{iPr}_3)Fe^{I}(N_2)$ (2) with H_2. The equilibrium study was conducted in an NMR tube with J-young valve. The relative concentrations of the two species involved in the equilibrium were determined by the integration of two hydride peaks at 10.0 and 8.0 ppm which represents $(SiP^{iPr}_3)Fe^{I}(N_2)$ and $(SiP^{iPr}_3)Fe^{I}(H_2)$, respectively; $K_{eq} = 50 \pm 20$ in C_6D_6 at room temperature.

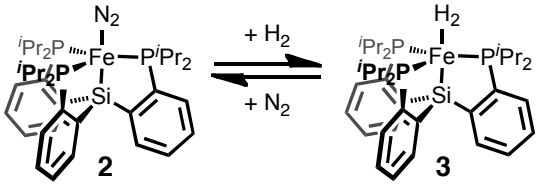

$$(SiP^{iPr}_3)Fe(N_2) + H_2 \longrightarrow (SiP^{iPr}_3)Fe(H_2) + N_2$$

$$K_{eq} = \frac{[FeH_2]\,[N_2]}{[FeN_2]\,[H_2]} = 50 \pm 20 \text{ at RT}$$

{(SiP$^{iPr}_3$)Fe(H$_2$)}{B(3,5-(CF$_3$)$_2$-C$_6$H$_3$)$_4$} (5). In an NMR tube with a J-young valve the green C_6D_6 /THF-d_8 (4/1) solution of **4** was degassed by three freeze-pump-thaw cycles on the Schlenk line resulting in an orange solution, indicative of {(SiP$^{iPr}_3$)Fe(THF)}{B(ArF)$_4$}. After H_2 gas (1 atm) was added the reaction mixture immediately changed color to gray at RT. ^{1}H-NMR reveals complete disappearance of **4** and the formation of **5**. ^{1}H-NMR (C_6D_6/THF-d_8 (4/1), ppm): 11.83, 8.2, 7.6, 5.87, 3.25, –4.67, –7.54. μ_{eff} (C_6D_6/THF-d_8 (4/1), 20°C): 3.4 μ_B. Satisfactory combustion analysis of **5** was not accomplished due to the lability of H_2 ligand. UV-Vis (THF, nm {cm^{-1}M^{-1}}): 590 {220}.

Equilibrium studies for the reaction of {(SiP$^{iPr}_3$)Fe(H$_2$)}{B(3,5-(CF$_3$)$_2$-C$_6$H$_3$)$_4$} (5) with THF. The equilibrium study was conducted by a UV-Visible spectroscopic technique using a Schlenk cuvette. The relative concentrations of the two species involved in the equilibrium were determined by the intensity of two bands at 505 ($\varepsilon \sim 2970$ cm^{-1}M^{-1}) and 755 ($\varepsilon \sim 315$ cm^{-1}M^{-1}) nm which represent {(SiP$^{iPr}_3$)Fe(N$_2$)}{B(3,5-(CF$_3$)$_2$-C$_6$H$_3$)$_4$} (**4**) and {(SiP$^{iPr}_3$)Fe(THF)}{B(3,5-(CF$_3$)$_2$-C$_6$H$_3$)$_4$}, respectively in THF; $K_{eq} = 2.1 \pm 0.4 \times 10^4$. The solubility of gases in THF at 101.33 kPa partial pressure of gas at 25 °C are 16.3 and 9.38 mM for N_2 and H_2, respectively obtained from the literature.[17]

[17] Gibanel, F; Lopez, M. C.; Royo, F. M.; Santafe, J.; Urieta, J. S. *J. Sol. Chem.* **1993**, *22*, 211-217

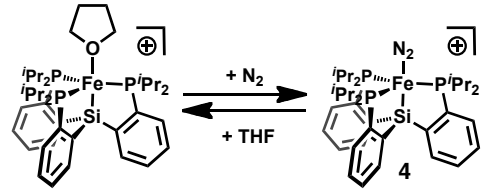

$$\{(SiP^{iPr}_3)Fe(THF)\}^+ + N_2 \longrightarrow \{(SiP^{iPr}_3)Fe(N_2)\}^+ + THF$$

$$K_{obs} = \frac{[Fe(N_2)^+]\,[THF]}{[Fe(THF)^+]\,[N_2]} = 2.1 \pm 0.4 \times 10^4 \text{ at RT}$$

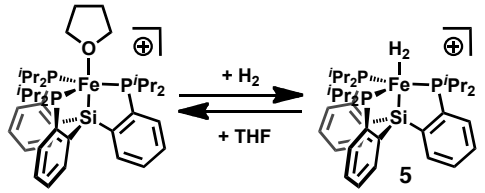

$$\{(SiP^{iPr}_3)Fe(THF)\}^+ + H_2 \longrightarrow \{(SiP^{iPr}_3)Fe(H_2)\}^+ + THF$$

$$K_{obs} = \frac{[Fe(H_2)^+]\,[THF]}{[Fe(THF)^+]\,[H_2]} = 1.9 \pm 0.4 \times 10^4 \text{ at RT}$$

Deprotonation of $\{(SiP^{iPr}_3)Fe(H_2)\}\{B(3,5\text{-}(CF_3)_2\text{-}C_6H_3)_4\}$ (5) with base.
$(SiP^{iPr}_3)Fe(N_2)(H)$ (6). **4** (14.6 mg, 9.4 μmol) and diisopropylethylamine (1.7 μL, 9.7 μmol) were charged into an NMR tube with a J-young valve with C_6D_6/THF-d_8 (ca. 0.4 mL/0.1 mL), yielding a green solution. The solution was degassed by 3 freeze-pump-thaw cycles, revealing an orange solution consistent with $\{(SiP^{iPr}_3)Fe(THF)\}\{B(ArF)_4\}$. H_2 (1 atm) was charged into the reaction mixture, yielding a transient gray solution (consistent with **5**) that immediately changed to orange-yellow upon mixing. The reaction was mixed overnight and solvent removed *in vacuo*. The yellow solid was extracted with pentane and the solvent removed *in vacuo* to yield **6** (5.1 mg, 88 %) as a yellow solid. ^{1}H-NMR (C_6D_6, ppm): 8.13 (2H, d, J = 7.2 Hz), 7.97 (1H, d, J = 7.2 Hz), 7.35 (3H, m), 7.2 (3H, m), 7.1 (3H, m), 2.78 (2H, m), 2.53 (2H, m), 2.30 (2H, m), 1.49 (6H, dd, J = 14, 6.8 Hz), 1.31 (6H, m), 1.21 (6H, dd, J = 12.4, 6.8 Hz), 0.94 (6H, dd, J = 12.4, 6.8 Hz), 0.80 (6H, s), 0.57 (6H, s), –13.8 (1H, dt, J = 83.2, 19.8 Hz). ^{31}P-NMR (C_6D_6, ppm, RT): 83 (br), 81 (s); (Tol-d_8, ppm, –80 °C): 98.05 (t, $^3J_{PP}$ = 180 Hz, $^3J_{PH}$ = 110 Hz), 79.5 (s), 67.4 (t, $^3J_{PP}$ = 180 Hz, $^3J_{PH}$ = 110 Hz). Crystals suitable for X-ray diffraction were obtained by slow evaporation of a benzene solution of **6**. Anal. Calcd. For $C_{36}H_{55}FeN_2P_3Si$: C, 62.42; H, 8.00; N, 4.04. Found: C, 61.99; H, 7.80; N, 3.85. UV-Vis (THF, nm {$cm^{-1}M^{-1}$}): 353 {3,360}, ~430 {sh}. IR (KBr pellet; cm^{-1}): 2061 ($^{14}N_2$) 1913 (H).

$(SiP^{iPr}_3)Fe^{II}(^{15}N_2)(H)$ (6-$^{15}N_2$). In a NMR tube with J-young valve the orange toluene-d_8 solution of **6** was degassed by three freeze-pump-thaw cycles on the Schlenk line. After $^{15}N_2$ gas (1 atm) was added the reaction was allowed to stand overnight at RT. Spectroscopic features in the ^{1}H-NMR were identical for **3**. ^{15}N-NMR (Toluene-d_8, ppm, at 293 K) 344 (dm, J = 4.1 Hz) and 331 (dd, J = 4.1, 2.0 Hz); free $^{15}N_2$ appears at 308.6 ppm. IR (KBr pellet; cm^{-1}): 1989 ($^{15}N_2$).

Figure S1. ^{1}H-NMR spectra of the reaction of **2** with H_2(g) in C_6D_6; (a) **2** (b) H_2 was added after three freeze-pump-thaw cycles (c) heated at 60°C for 6 hrs (d) degassed by three freeze-pump-thaw cycles (e) overnight under full vacuum (f) N_2 was added.

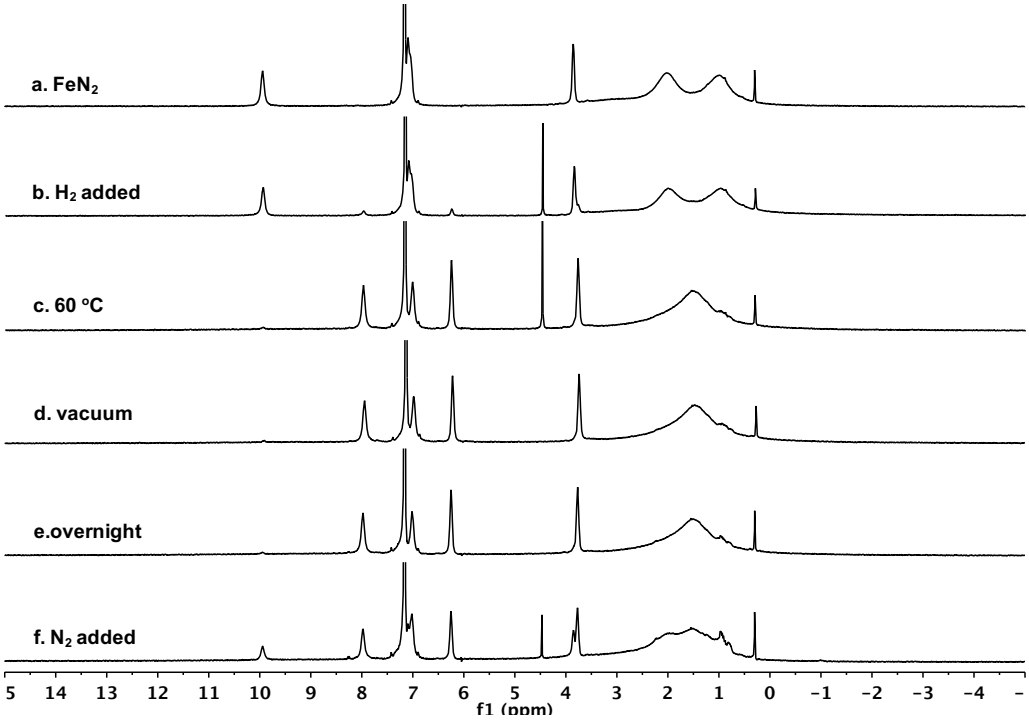

Figure S2. ^{1}H-NMR spectra of the reaction of **2** with H_2(g) in Toluene-d_8; (a) **2** (b) H_2 was added after three freeze-pump-thaw cycles (c) heated at 60°C for 6 hrs (d) degassed by three freeze-pump-thaw cycles (e) N_2 was added.

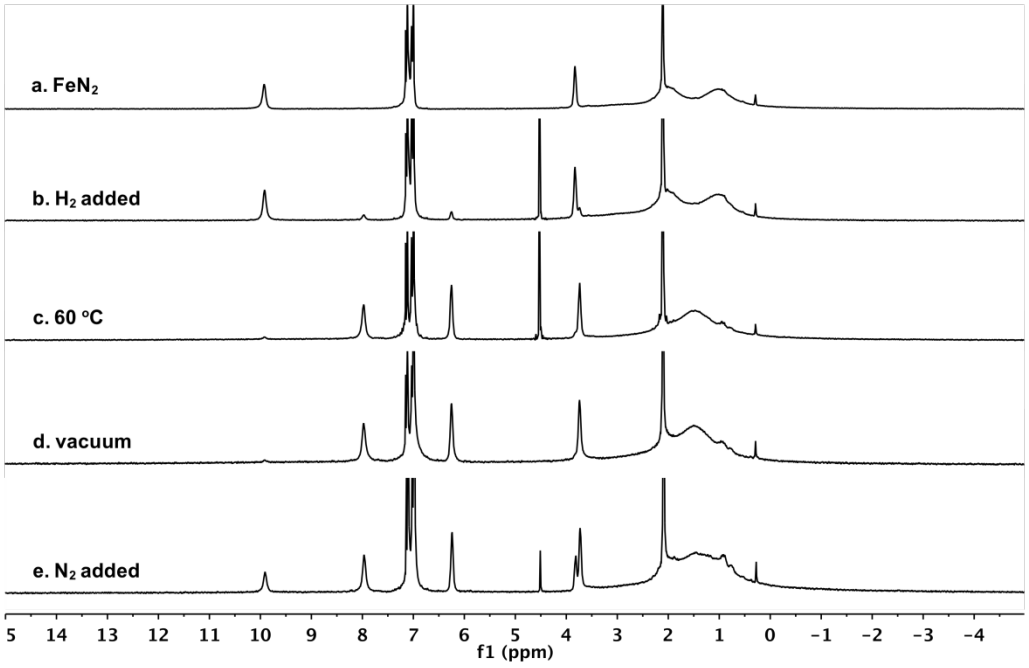

Figure S3. UV-Vis spectra (top) and near IR (bottom) (nm {$cm^{-1}M^{-1}$}) of **3**, blue spectra: 290 {8,200}, 380 {4,450}, 1,350 {100}) and **2**, red spectra: 300 {>12,900}, 400 {5,600}, 1,250 {300}) in toluene at RT.

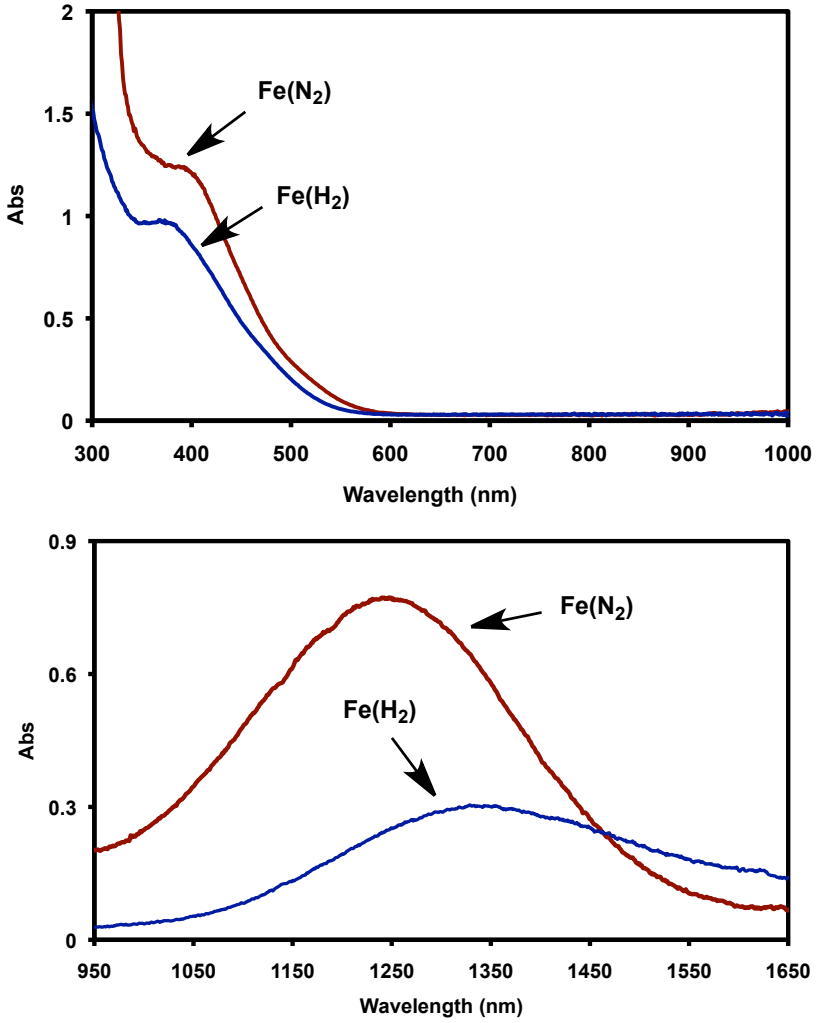

Figure S4. React IR spectra (cm^{-1}) of the reaction of **2** (red spectra) with H_2 (g) in THF at RT. The spectra were collected for 22 hrs with an interval of 1 hr.

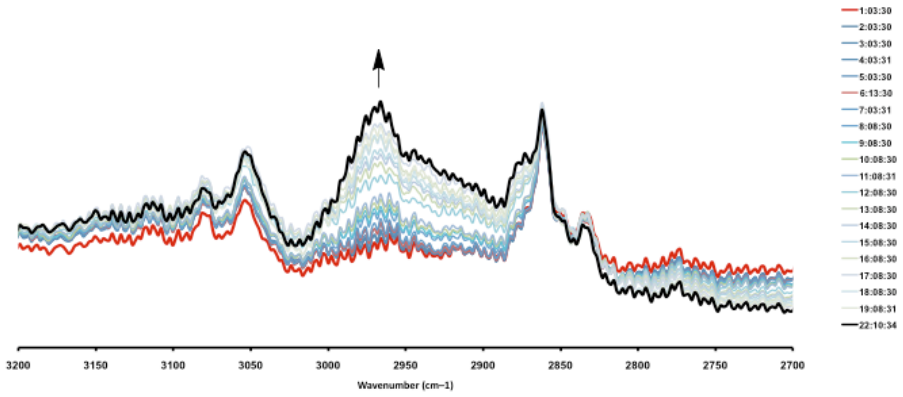

Figure S5. ^{1}H-NMR spectra of **3** in C_6D_6; (a) in-situ generated **3**, (b) a powder sample of **3** dissolved in C_6D_6.

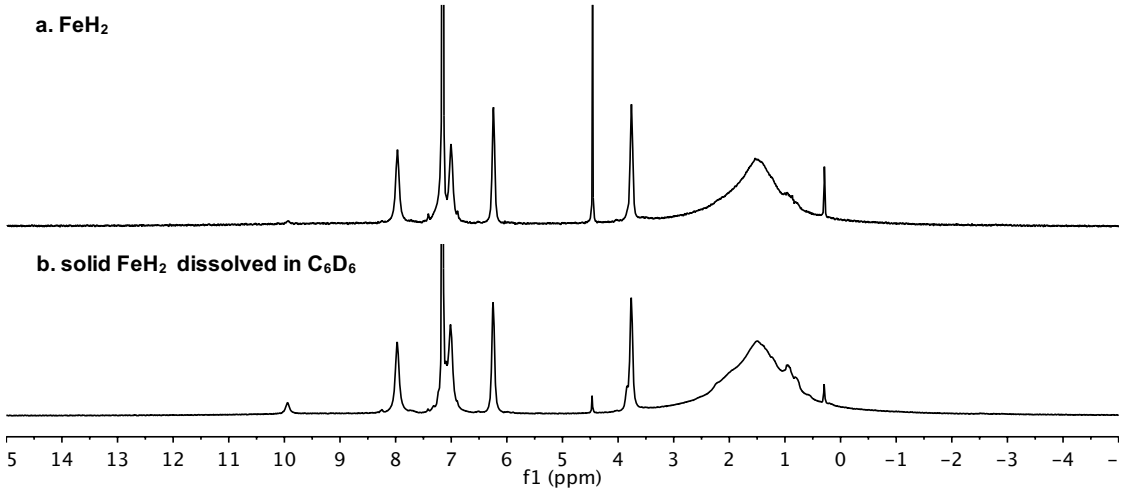

Figure S6. ^{1}H-NMR spectra of the reaction of **2** with D_2 (g) in C_6D_6; (a) complex **2** (b) spectrum after D_2 was added after three freeze-pump-thaw cycles (c) spectrum after shaking under D_2 overnight at RT (d) spectrum after degassing and then adding H_2 (g).

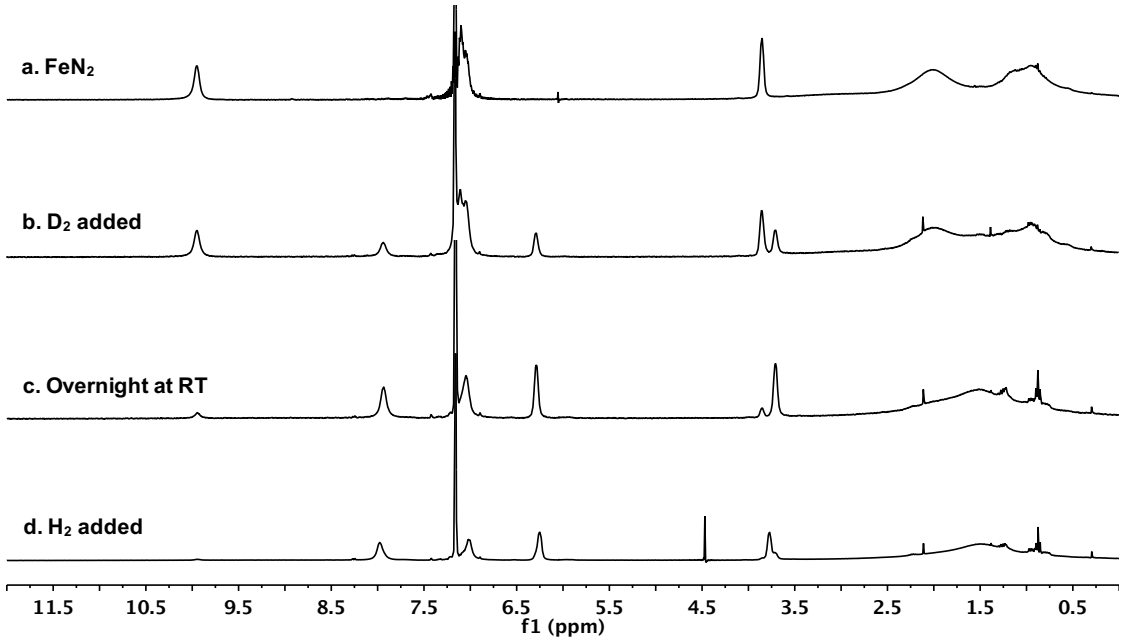

Figure S7. ^{2}H-NMR spectra of **3-D$_2$** in toluene-d_8; (a) D_2 (g), (b) **3-D$_2$** at RT, (c) **3-D$_2$** at –70°C.

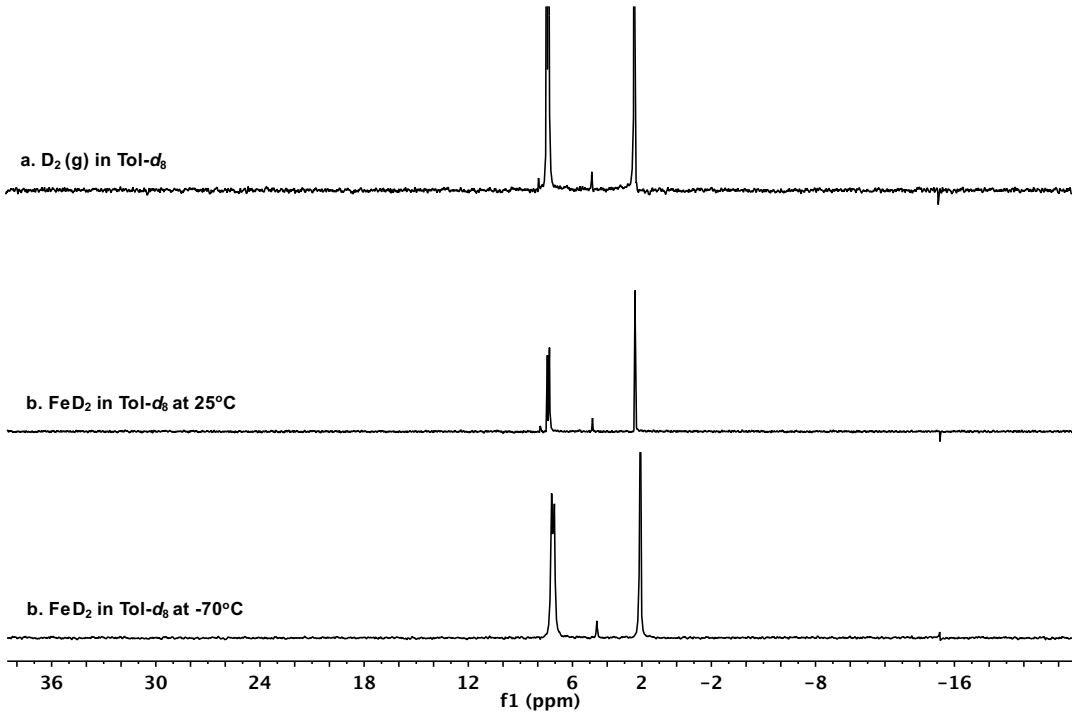

Figure S8. ^{1}H-NMR spectra of the reaction of **2** with HD (g) in C_6D_6; (a) **2** (b) HD was added after three freeze-pump-thaw cycles (c) shaken for 11 hrs at RT (d) shaken for 15 hrs at RT. Inset: 4-5 ppm region showing one singlet peak at 4.43 ppm for H_2 (g) and one triplet peak at 4.39 ppm for HD (g). H_2/HD ratios are 0.12, 0.15 and 0.17 for b, c, d, respectively.

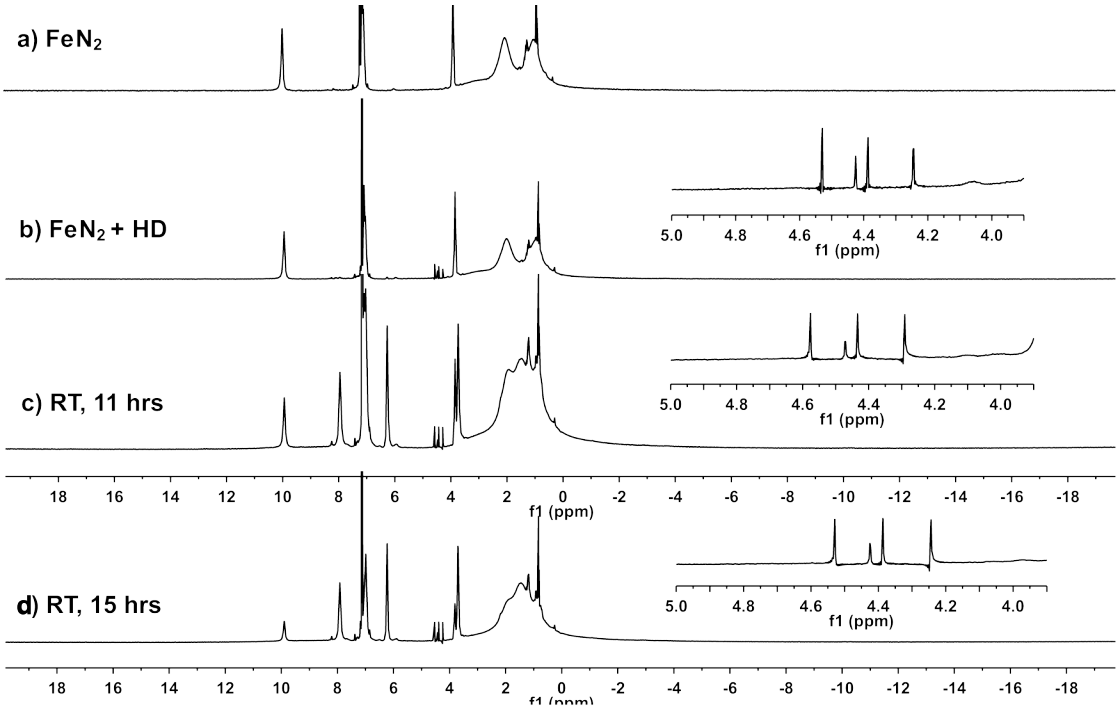
a) FeN2
b) FeN2 + HD
c) RT, 11 hrs
d) RT, 15 hrs
f1 (ppm)

Figure S9. Solid-state structure of **3** obtained from a benzene solution of **3** under vacuum for several weeks. Hydrogen atoms from the $[SiP^{iPr}_3]^-$ ligand are omitted for clarity.

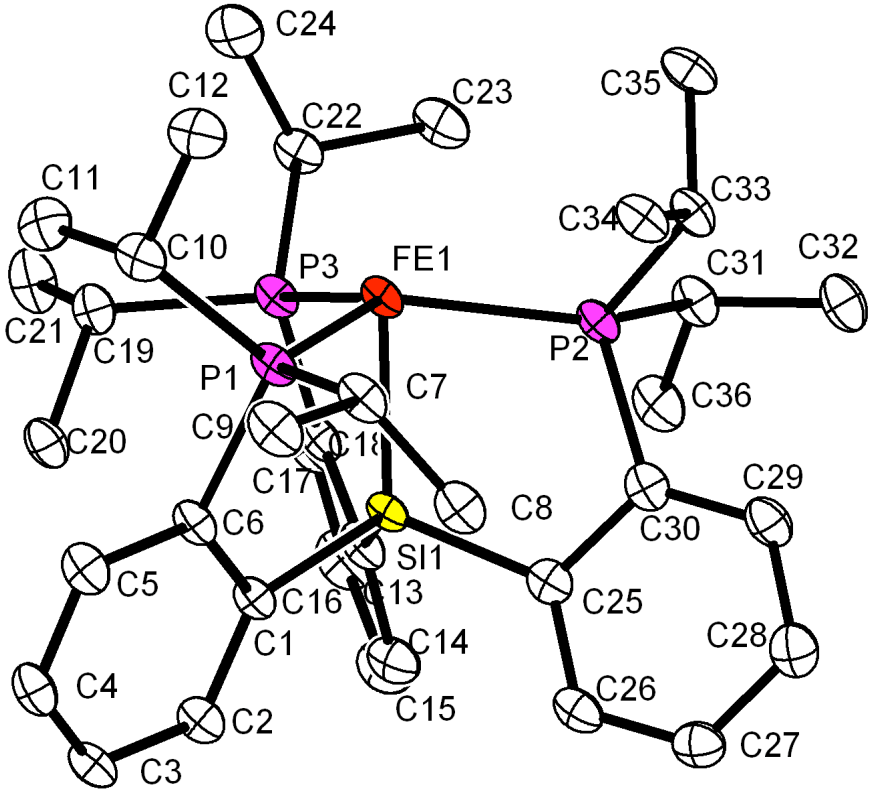

Figure S10. Solid-state structure of **3** obtained from a saturated benzene solution of **3** under an H_2 atmosphere for several days. Hydrogen atoms from the $[SiP^{iPr}_3]^-$ ligand are omitted for clarity.

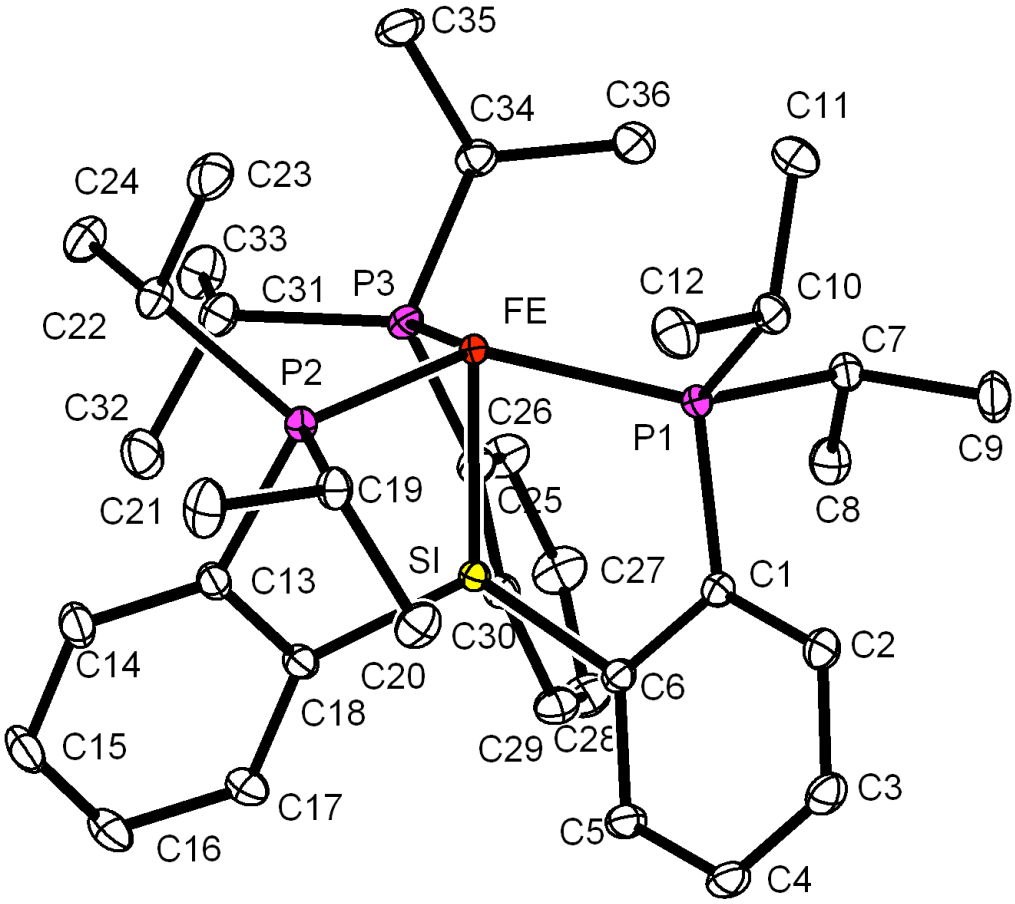

Figure S11. X-band EPR data of (A) **2**, (B) **3**, (C) **3′** and (D) a mixture of **2** and **3** in THF/2-MeTHF (9/1) at 77 K.

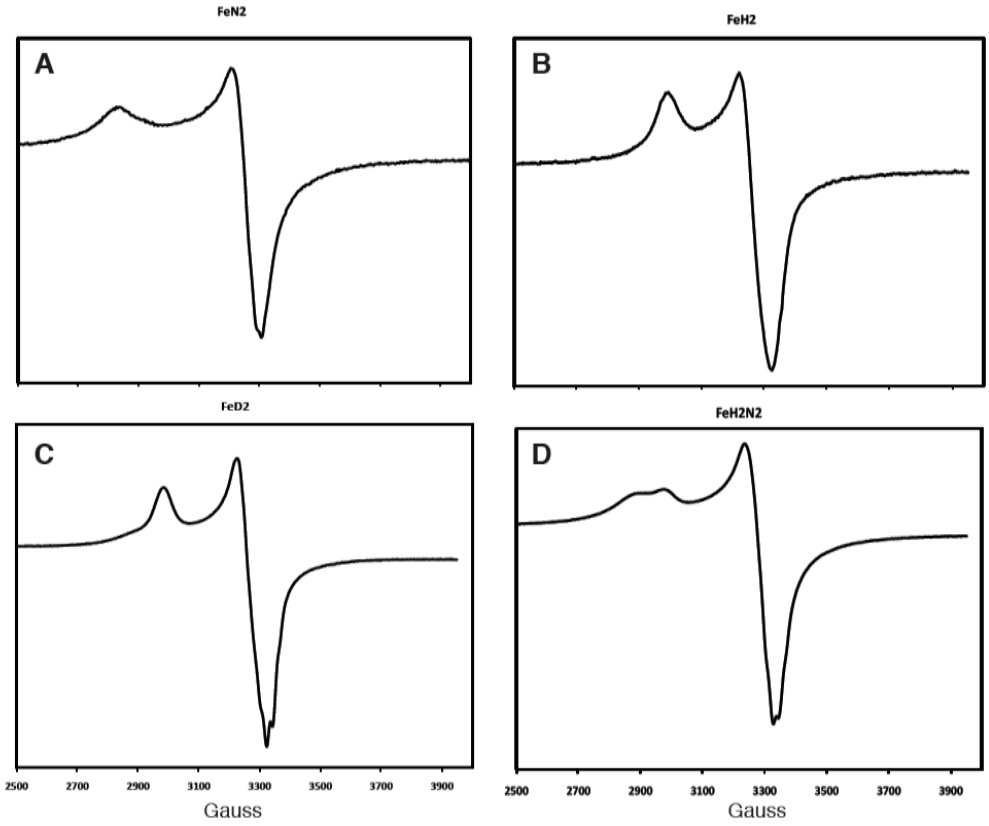

Figure S12. X-band EPR data of **3′** in THF/2-MeTHF (9/1) (blue), and in toluene (red), at 20 K.

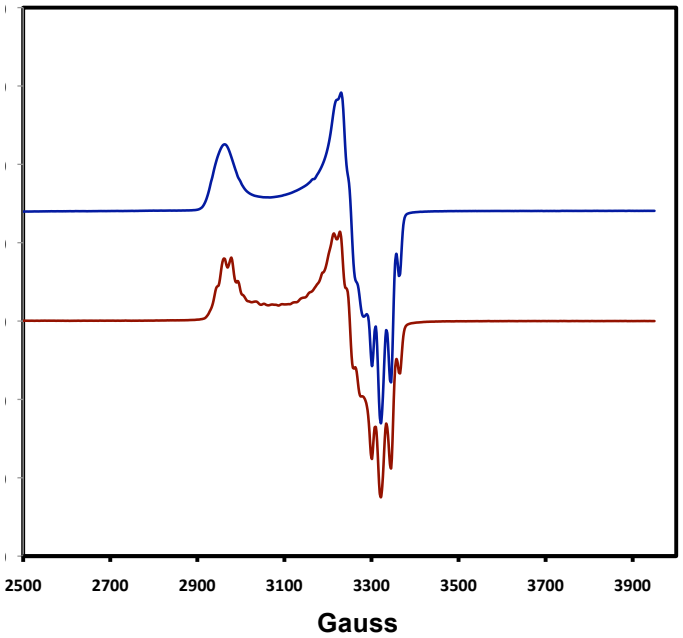

Figure S13. X-band EPR spectra of **2**, **3**, and **3′** in toluene at 20 K.

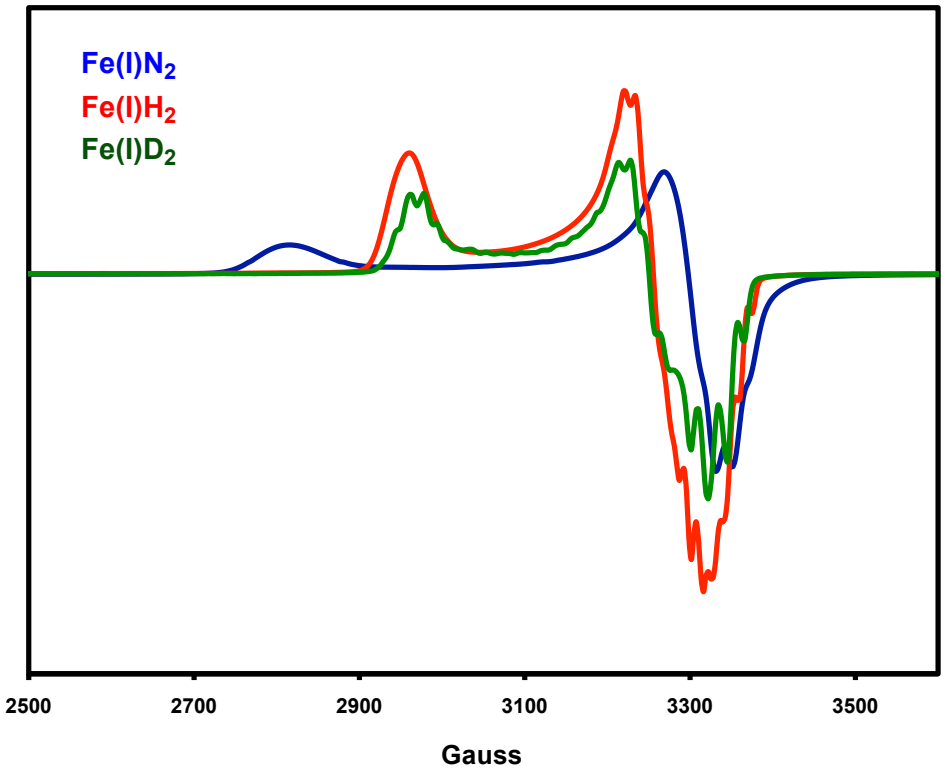

Figure S14. Experimental (blue) and simulated (black) EPR spectra of **2** in toluene at 20 K.

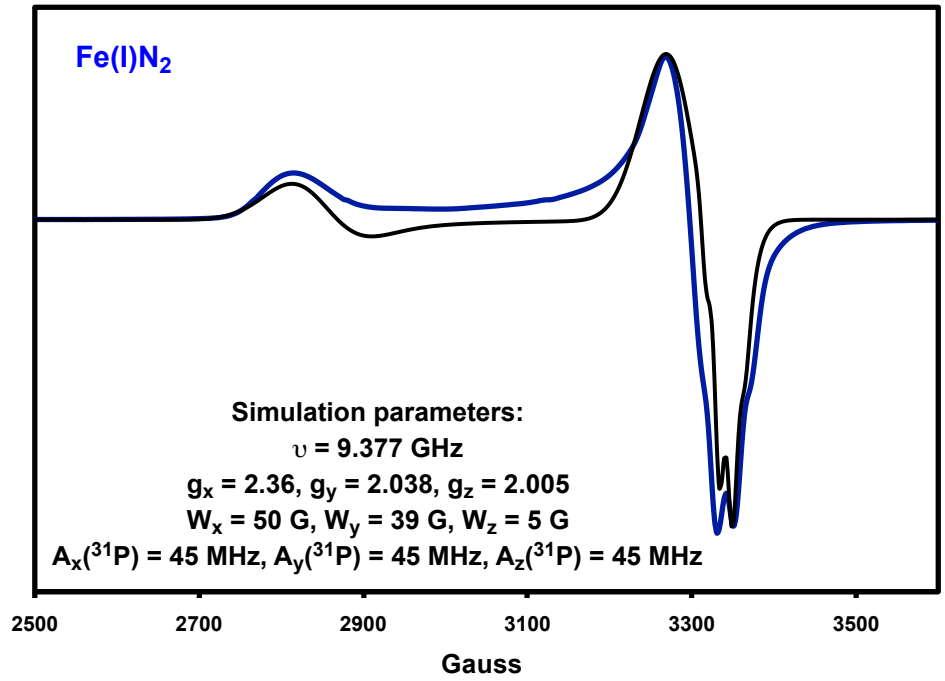

Figure S15. Experimental (red) and simulated (black) EPR spectra of **3** in toluene at 20 K.

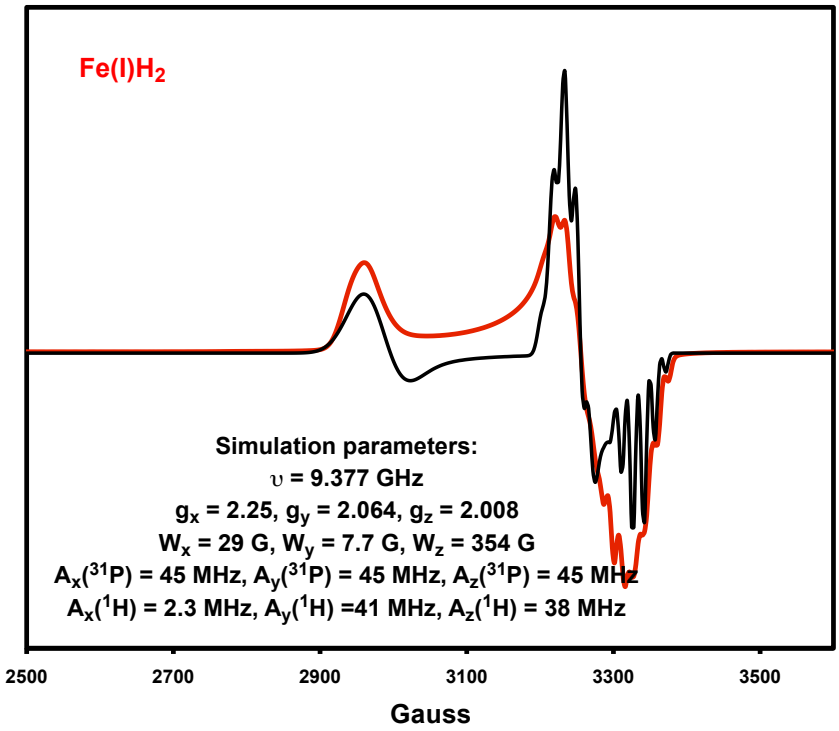

Figure S16. Experimental (green) and simulated (black) EPR spectra of **3′** in toluene at 20 K.

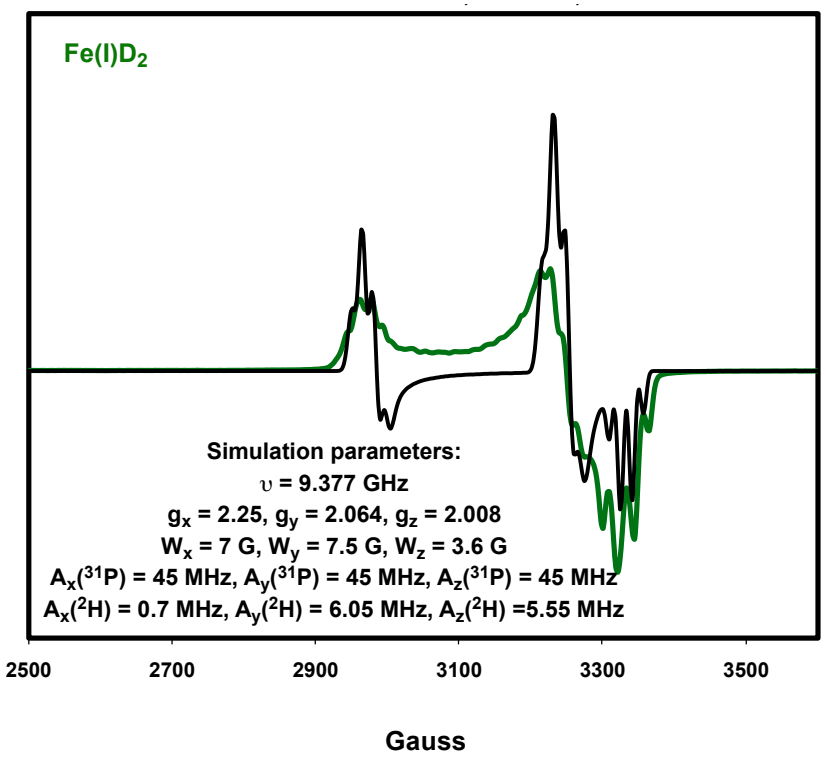

Figure S17. EPR spectra of **3** in frozen solution (35 GHz, 9 GHz), and in powder (9 GHz).

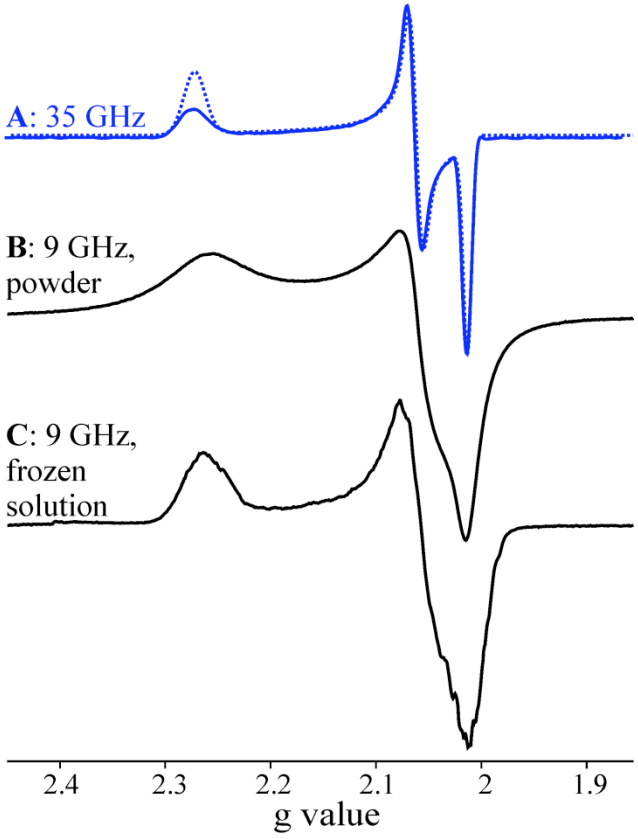

The EPR spectra of A) the frozen solution of **3** in THF/2-MeTHF (9/1) at 35 GHz (solid blue line) with corresponding simulation (dotted blue line); B) the powder of **3** at 9 GHz; and C) the frozen solution of **3** at 9 GHz. The frozen solution EPR spectrum of **3** at 9 GHz shows partially resolved hyperfine splitting from the three ^{31}P nuclei of the $[SiP^{i}Pr_3]^-$ ligand.

Figure S18. 2D field-frequency ^{1}H ENDOR pattern of **3** in frozen solution with ENDOR simulations corresponding to $\beta = 0^{o}$, 15^{o}, and 30^{o}.

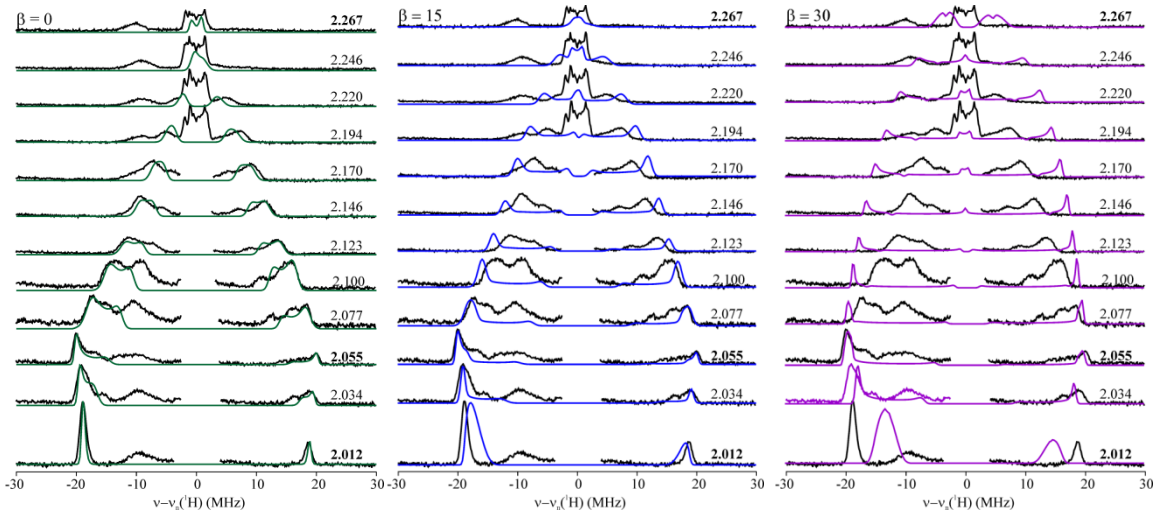

35 GHz stochastic 2D field-frequency CW ENDOR pattern for **3** (black) with simulations of the exogenous 'H_2' ^{1}H ENDOR response corresponding to structural models characterized by different values of the angle β: mono-hydride and rotating H_2, 0^{o}; static H_2, 15^{o}; and di-hydride, 30^{o}. *Experimental conditions.* Microwave frequency, 35.272 GHz; modulation amplitude, 0.66 G; temperature, 2 K; stochastic sequence (delay/sample/RF), 0.75/1/1 ms; rf excitation was randomly hopped and broadened to 100 kHz. *Simulations*. **g** = [2.267, 2.059, 2.01]; **A** = +[2.3, -40.6, 37.8] MHz; $\alpha = \gamma = 0$ (g_1 = z); EPR/ENDOR linewidth, 300/0.5 MHz; simulation intensities individually matched at each field position.

Figure S19. Single-crystal EPR analysis of **3**.

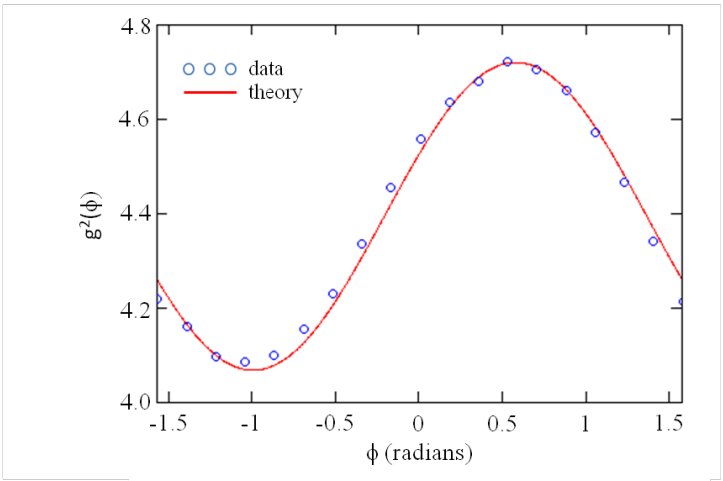

The angle dependence of g^2 for a single crystal in an arbitrary orientation is rotated around an axis normal to the external magnetic field. $\phi = 0^o$ represents an arbitrarily chosen initial crystal direction normal to the external field. Open blue dots represent the measured values of g^2 as a function of rotation angle. The data was fit to eqn. 5 in Gurbiel et al, and modeled using the frozen solution principle g-values as described in the experimental section above. The solid red line represents the calculated dependence of $g^2(\phi)$ as derived from the fit.

Figure S20. ^{1}H PESTRE trace of **3** at g_2.

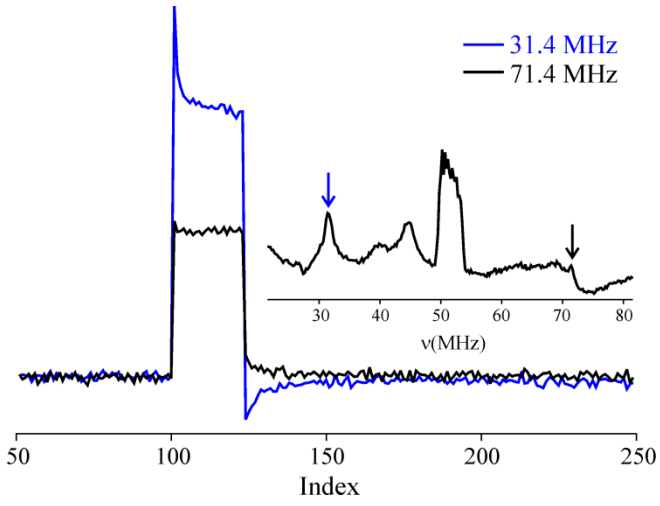

PESTRE spectra measured from **3** at the ν_+ (71.4 MHz; black) and ν_- (31.4 MHz; blue) frequencies from the ^{1}H ENDOR response at $g_2 = 2.06$. *Inset*. Davies ^{1}H ENDOR spectrum at g_2. The frequencies at which a PESTRE spectrum is acquired are denoted by arrows. *Conditions*. PESTRE: microwave frequency, 34.92 GHz; π = 200 ns; τ = 600 ns; repetition rate, 30 ms; t_{rf} = 30 μs; RF frequency, 71.4 MHz (ν_+) and 31.4 MHz (ν_-); t_{mix} = 5 μs; ^{1}H ENDOR: π = 200 ns; τ = 600 ns; repetition rate, 10 ms; t_{rf} = 30 μs; RF frequency randomly hopped.

Figure S21. ^{2}H ENDOR field-frequency pattern with simulations for **3′**.

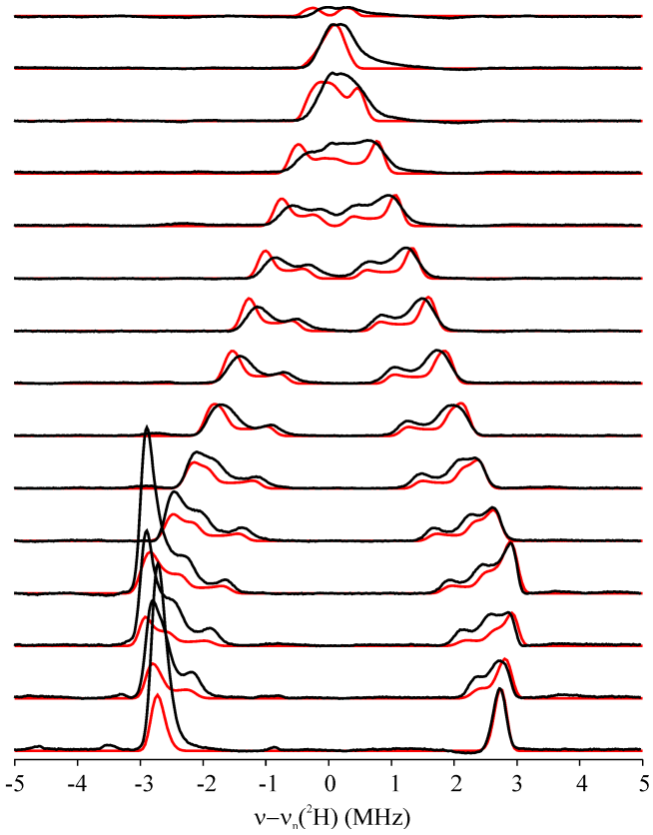

35 GHz stochastic 2D field-frequency CW ENDOR pattern for **3′** (black) with simulations of the exogenous '$^{2}H_2$' ^{2}H ENDOR response (red). A linear baseline was fit individually to each spectrum and then subtracted. *Experimental conditions*. Microwave frequency, 35.388 GHz; microwave power, 0.1 mW; temperature, 2K; modulation amplitude, 0.66 G; RF was swept from low to high frequency and broadened to 50 kHz. *Simulations*. **g** = [2.267, 2.059, 2.01]; **A** = +[0.7, -6.05, -5.55] MHz; (α,β,γ) = (0,7,0); **P** = [-0.05, -0.02, -0.03] MHz; (α,β,γ) = (0,0,0); EPR/ENDOR linewidth, 150/0.15 MHz.

Figure 22. DFT optimized geometries of **3** and FeH^-/SiH^+.

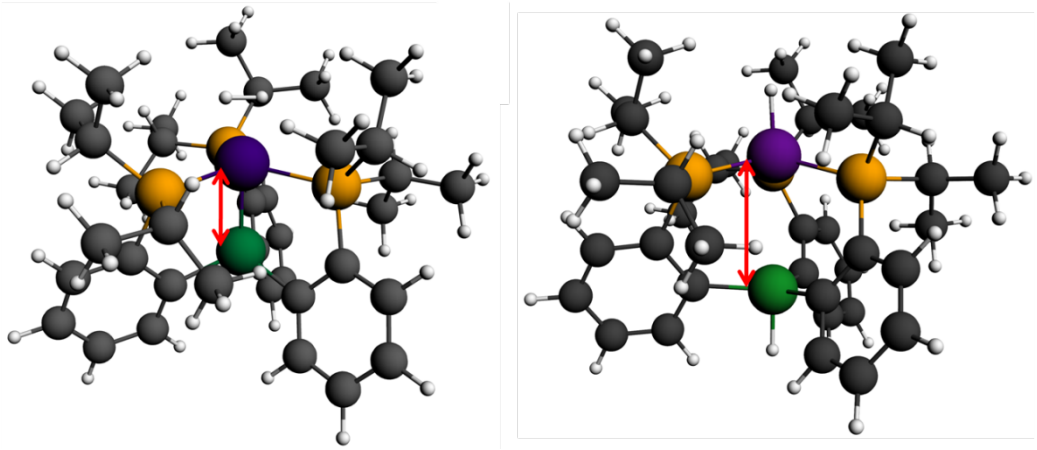

DFT-optimized geometry for **3** (*left*) and FeH^-/SiH^+ (*right*), the proposed product of heterolytic cleavage of H_2. The distance between Fe and Si increases from 2.25 to 3.28 Å upon protonation of Si. See experimental section above for computational details. Color legend: Fe, purple; Si, green; C, black; P, yellow; H, white.

Figure S23. ^{1}H-NMR spectra of **4** (top), {(SiP$^{i\mathrm{Pr}}_3$)Fe(THF-d_8)}{B(3,5-(CF$_3$)$_2$-C$_6$H$_3$)$_4$} (middle), and **5** (bottom) in C_6D_6/THF-d_8 (4/1) at room temperature.

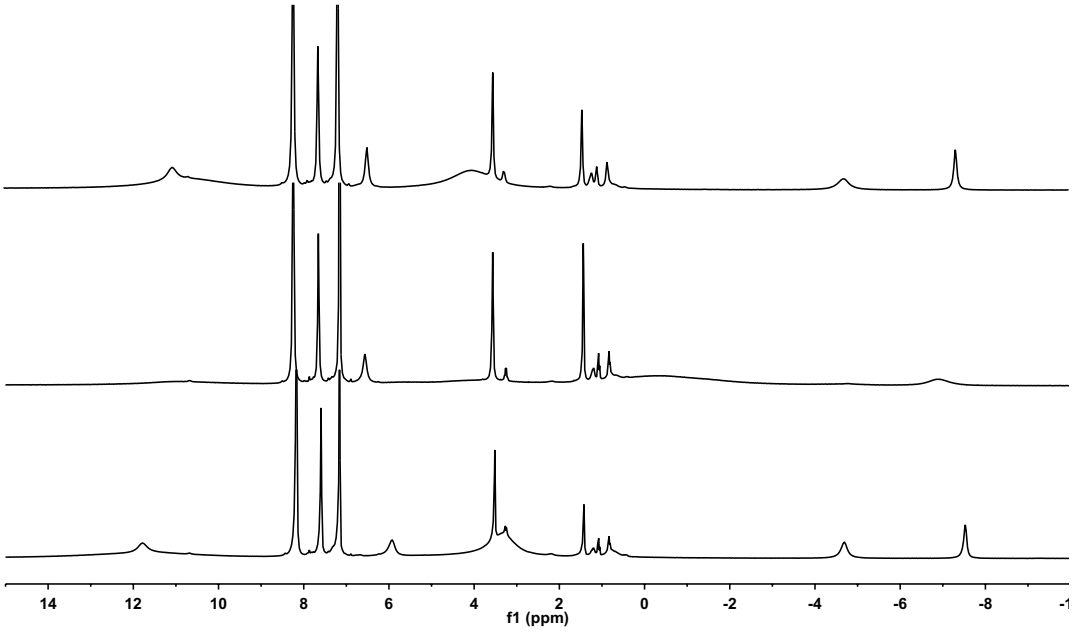

Figure S24. ^{1}H-NMR spectra of A: **4**, B: with N_2/H_2 (5:1), C: with N_2/H_2 (1:1), D: with N_2/H_2 (1:5) and E: **5** in C_6D_6/THF-d_8 (4/1) at room temperature.

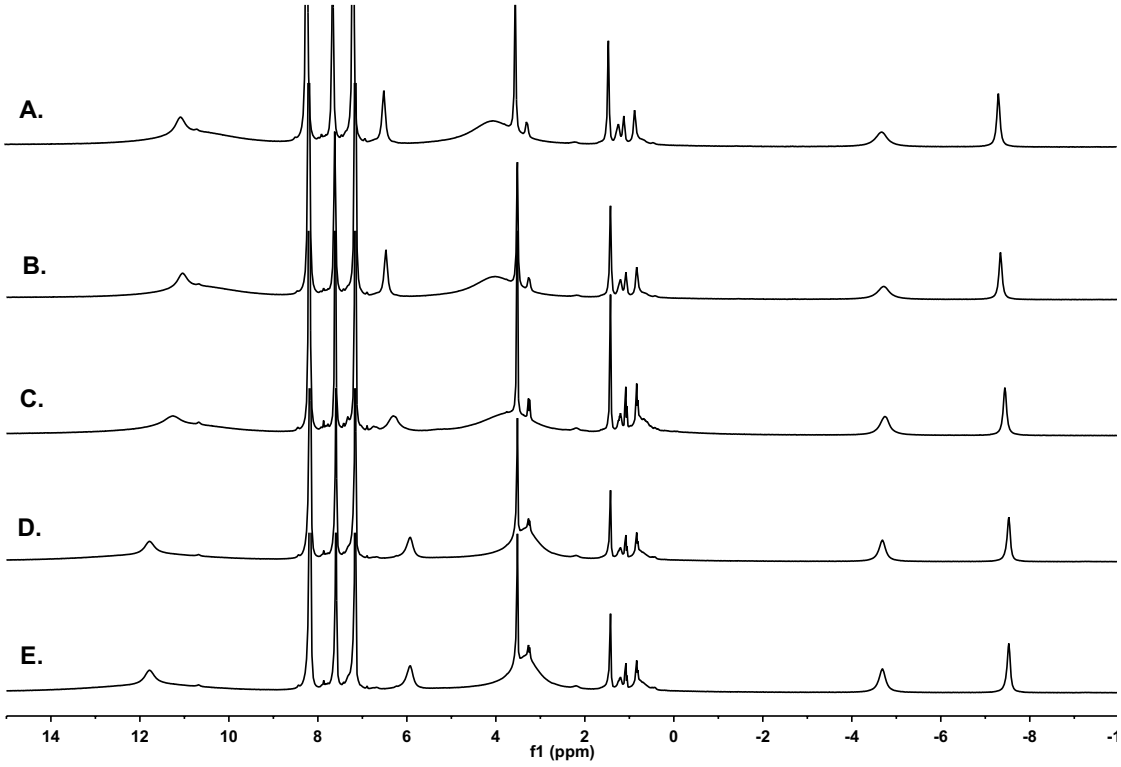

Figure S25. UV-Vis spectra of a series of $\{(SiP^{iPr}_3)Fe(L)\}\{B(3,5\text{-}(CF_3)_2\text{-}C_6H_3)_4\}$; L = N_2, THF, and H_2 in tetrahydrofuran at room temperature; a: $\{(SiP^{iPr}_3)Fe(N_2)\}\{B(3,5\text{-}(CF_3)_2\text{-}C_6H_3)_4\}$ (**4**), b: $\{(SiP^{iPr}_3)Fe(THF)\}\{B(3,5\text{-}(CF_3)_2\text{-}C_6H_3)_4\}$ produced from applying full vacuum by freeze-pump-thaw cycles, c: $\{(SiP^{iPr}_3)Fe(H_2)\}\{B(3,5\text{-}(CF_3)_2\text{-}C_6H_3)_4\}$ (**5**) generated from a addition of H_2 (g), d: $\{(SiP^{iPr}_3)Fe(THF)\}^+$ produced from applying full vacuum, e: a mixture of **4**, $\{(SiP^{iPr}_3)Fe(THF)\}^+$ and **5** produced by addition of H_2/N_2 (1/2) mixture.

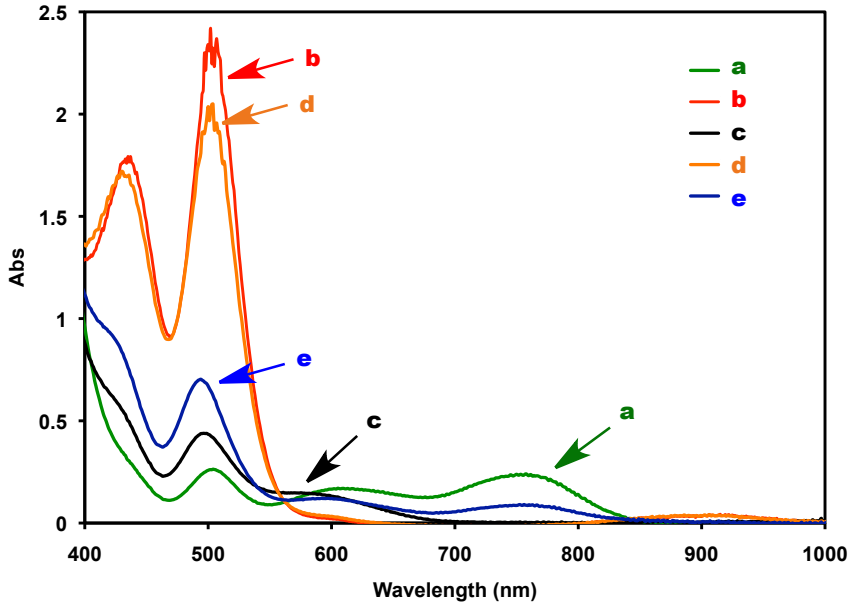

Figure S26. UV-Vis spectrum (nm $\{cm^{-1}M^{-1}\}$) of $\{(SiP^{iPr}_3)Fe(N_2)\}\{B(3,5\text{-}(CF_3)_2\text{-}C_6H_3)_4\}$ (**4**, green spectra: 613 {260}, 757 {330}) in diethyl ether at room temperature. After applying full vacuum by freeze-pump-thaw cycles a new species was grown (blue spectra: 504 {> 460}, 580 {> 910}).

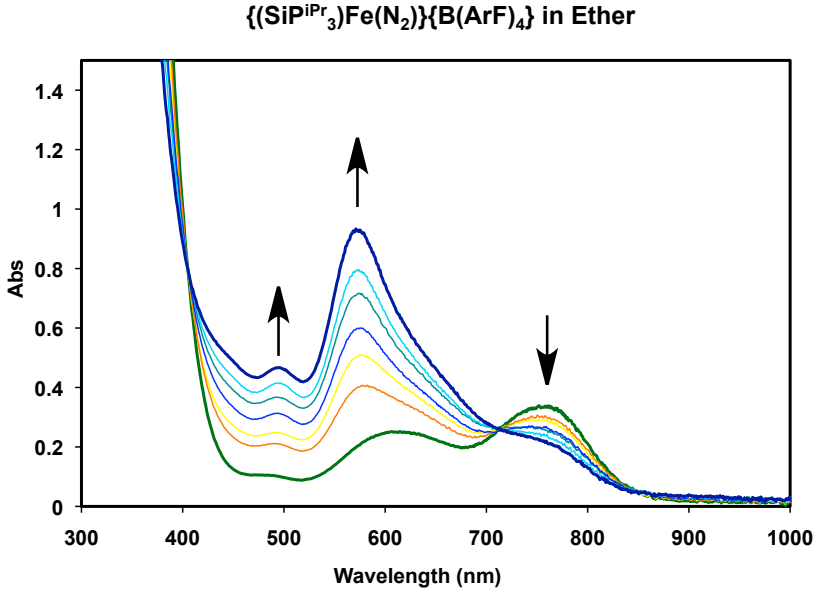

Figure S27. ^{1}H-NMR spectrum of **6** in toluene-d_8 at RT.

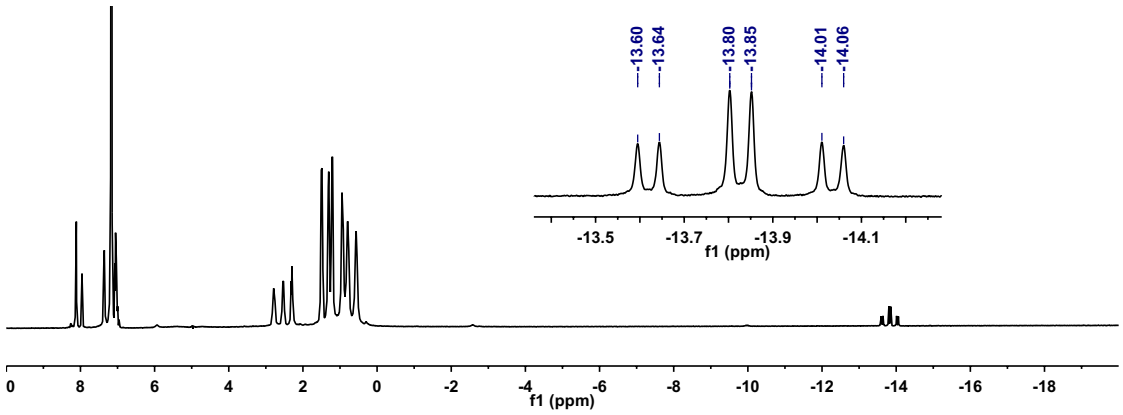

Figure S28. ^{15}N-NMR spectrum of **6** with ^{31}P-decoupling measured at 293 K; 344 (dm, J = 4.1 Hz) and 331 (dd, J = 4.1, 2.0 Hz) ppm; free $^{15}N_2$ appears at 308.6 ppm in toluene-d_8.

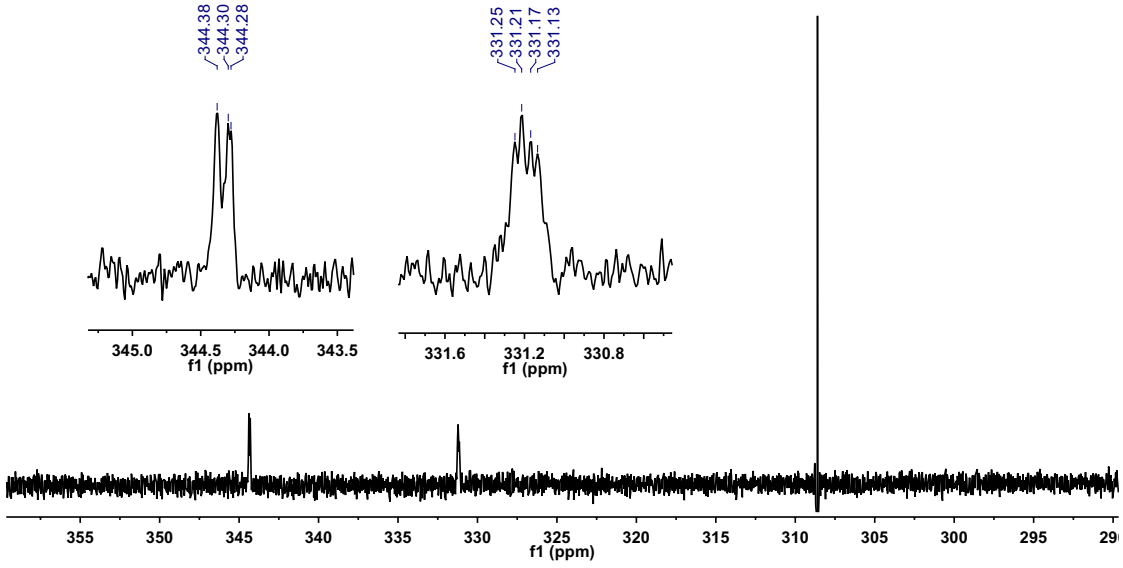

Figure S29. Variable temperature ^{31}P-NMR spectra of **6** in toluene-d_8.

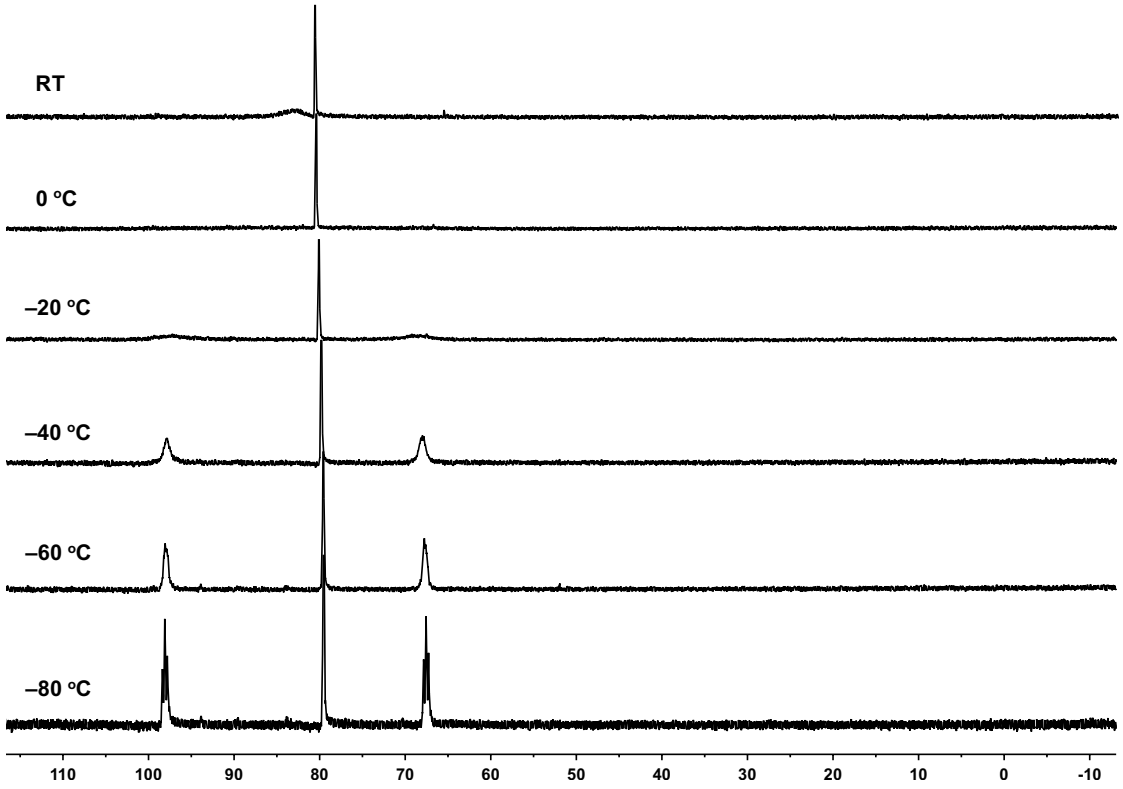

Figure S30. ^{31}P-NMR spectrum of **6** in toluene-d_8 at –90°C.

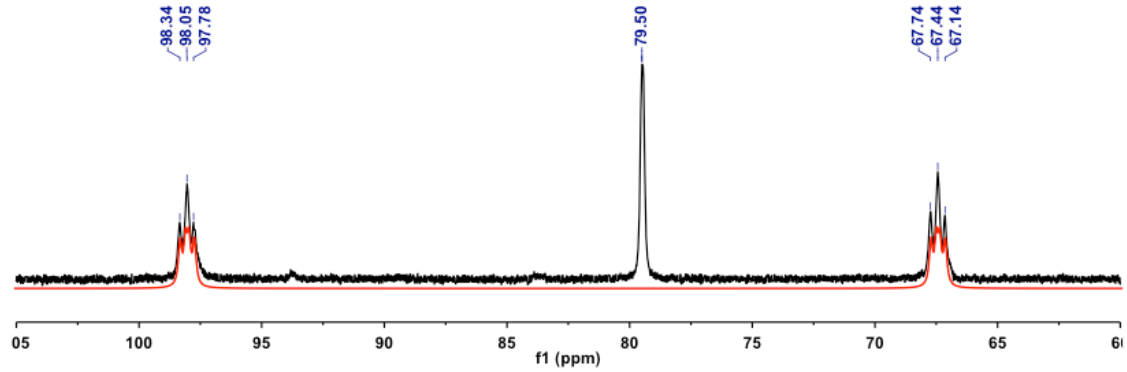

Figure S31. Solid-state structure of $(SiP^{iPr}_3)Fe(N_2)(H)$ (**6**). All C-H hydrogen atoms are omitted for clarity. Fe-H hydrogen was located on the Fourier difference map and its position was freely refined.